COMMUNICATIONS IN SCIENCE AND TECHNOLOGY
Homepage: cst.kipmi.or.id

Novel colored biomass-waste from food industry sector derived hierarchical porous carbon nanofiber for robust symmetric supercapacitor

Wan Mery Nursyaputri[a], Zeeva Khalilah Fairuzy[b], Zahra Khumairah[c], Novi Yanti[d,f], Nursyafni Nursyafni[d], Apriwandi Apriwandi[d], Rika Taslim[e,*], Erman Taer[d,*]

[a]*Madrasah Aliyah Negeri 3 Pekanbaru City 28293, Indonesia*
[b]*Department of Medical Education, University of Riau 28133, Indonesia*
[c]*Department of Biology, University of Brawijaya 65145, Indonesia*
[d]*Department of Physics, University of Riau 28293, Indonesia*
[e]*Department of Industrial Engineering, Universitas Islam Negeri Sultan Syarif Kasim, Riau 28293, Indonesia*
[f]*Energy Research and Nano Carbon Center, Riau 28293, Indonesia*

Article history:
Received: 12 September 2024 / Received in revised form: 13 December 2024 / Accepted: 15 December 2024

Abstract

A major challenge in the use of supercapacitor energy storage applications is optimizing 3D-hierarchical porous and 2D nanofiber structures to improve the electrochemical performance of colored biomass-derived activated carbon (AC). Therefore, this study aims to synthesize AC from Dracaena Angustifolia (DA) leaves and dregs using a sustainable method through chemical activation and high-temperature pyrolysis. AC was designed to be adhesive-free to maintain the true mechanical properties of the precursor. Research results showed that the sample of DA-dregs-KOH shows optimal results with a specific surface area (317.66 m^2 g^{-1}). The electrochemical performance of hierarchical porous carbon treated with 1 M H_2SO_4 electrolyte in a 2-electrode system had a nanofiber structure with the highest specific capacitance (248 F g^{-1}) at 1 A g^{-1} and energy density (12.96 Wh kg^{-1}) with a coulomb efficiency 84.1%. Based on these results, DA dreg-KOH based porous AC with hierarchical porous morphology shows significant potential to be used as binder-free electrode materials that can produce high-performance supercapacitors as a new renewable and sustainable energy storage solution.

Keywords: Colored_biomass; hierarchical_porous; nanofiber; electrode materials; supercapacitor

1. Introduction

In recent years, the world has been facing several problems associated with global warming, energy scarcity, and environmental damage [1]. Therefore, environmentally friendly solutions are needed to find raw materials in the energy sector as an alternative to fossil fuels [2]. An effective alternative in this context is the use of natural materials based on biomass waste as a sustainable and renewable source due to their abundance [3]. Examples of reliable biomass waste include remains of animals, plants, or other microorganisms [4]. Recent reports have also shown an increased interest in using materials to produce porous activated carbon (AC) with high carbon purity, large surface area, and optimal pore size distribution.

Based on previous results, the supercapacitor is an electronic device that can be used to store electrical charges with high power density [5]. This device is commonly used to convert biomass waste into activated carbon through a simple, environmentally friendly, and low-cost method [6]. Barley, shrimp [7], hemp seed hull [8], paddy straw [9], reed straw [10], chitin [11], kraft, organosolv [12], and others are examples of biomass waste that have been studied and confirmed to have promising results as a carbon source [13]. Moreover, those with natural color content are believed to produce additional pore structures when pyrolyzed at high temperatures [14]. One of the potential biomass waste from the food industry sector, which is common and known in several countries is Suji leaves waste (Dracaena Angustifolia Roxb/DA.).

Several studies have shown that Suji leaves have a rich green color from the chlorophyll pigment stored in the lamella organelles. The chlorophyll in the plant is intricately connected to form a basic tetrapyrrole ring network with methine (-C=), which binds magnesium and is hydrophobic. The total chlorophyll a/b of Suji leaves is higher compared to other plants and is characterized by a deeper green color. The

* Corresponding author.
Email: erman.taer@lecturer.unri.ac.id
https://doi.org/10.21924/cst.9.2.2024.1534

green color is often used as a natural coloring in ingredients for making various types of food. The leaves can also be processed into dregs with a pheophytin structure, which loses Mg metal and becomes waste for the environment [15]. Processing the dregs into supercapacitor electrodes is an alternative method that can provide useful and economic value from waste. Suji leaves contain chlorophyll, essential oils, saponins, alkaloids, flavonoids, and tannins, which have significant potential as a source of porous carbon for basic electrode materials [16]. Where, activated carbon from biomass materials can provide empty spaces or micro-nano-scale pores in their precursors.

According to previous research, organic essential oil content is an odorous volatile substance that can provide empty spaces as a source of porous carbon when given heat treatment at high temperatures. Where the resulting porosity can support the performance of supercapacitor electrodes in storing electrical charges. This result is in line with [17] who processed mushroom waste rich in carbon elements (53.7%) with KOH into AC with a high surface area (1116 m^2 g^{-1}) for supercapacitor electrode. [6] has also created a supercapacitor with a storage capacity of 268 F g^{-1} and high specific energy (18.6 Wh kg^{-1}) based on ginseng coffee waste through KOH chemical activation. In addition, KOH has been proven to be effective in the formation of pore structure and increase in surface area [13]. Previous studies have also shown its ability to maintain and produce fiber-like nanoporous structures, which support the optimization of supercapacitor electrode conductivity [18].

In this study, experiments and performance tests were carried out on a supercapacitor made from Suji leaves dregs. The results are very useful in comparing the characteristics of Suji leaves-based AC and Suji leaves waste for supercapacitor electrodes through 0.5 M KOH impregnation. Electrode preparation was packaged as a solid monolith without the use of additional adhesives, employing a complex non-template technique. High-quality AC with almost the same variation of DA dregs-KOH was prepared using expensive and abundantly available graphene or wood waste with a surface area of 317.66 m^2 g^{-1} and a high specific capacitance of 248 F g^{-1}. The use of DA biomass, with its high chlorophyll content and potential for hierarchical porosity, presents a novel and sustainable source for supercapacitor electrodes.

2. Materials and Methods

2.1. Preparation

An effective, efficient, and environmentally friendly method was selected for processing Suji leaves and dregs. This was conducted to produce hierarchical porous activated carbon as the primary material for supercapacitor electrodes. Furthermore, the investigation focused on the effect of color from chlorophyll pigments in increasing the purity of non-template activated carbon. The following is shown in Fig. 1, the conversion flow of suji leaf waste into activated carbon electrodes with a hierarchical pore structure for supercapacitors. First, 5 kg of Suji leaves were carefully prepared and thoroughly cleaned. A total of 3 kg of leaves were squeezed while the chlorophyll pigment was removed to obtain Suji dregs. Meanwhile, the remaining 2 kg of Suji leaves were immediately cut into smaller pieces (3-5 cm). Second, the prepared Suji leaves and dregs were dried in the sun for approximately 3 days. Subsequent drying used a 110 ºC drying oven (electrical warmer BERJAYA ISO 9001: 2000) until the mass shrinkage was <6%. Third, 30g of each sample was converted into carbon through a precarbonization process using a 250 ºC vacuum oven for 2.5 hours. Fourth, 2 carbon particles from each sample were crushed mechanically using a pestle and mortar. The process of refining carbon particles to the micrometer scale was continued using a ball milling tool in a vacuum tube for 20 hours. Fifth, uniformity of carbon particle size was performed through manual sieving 60 µm. Sixth, Suji carbon powder and dregs were each chemically activated using potassium hydroxide (KOH, 0.5 M). The chemical impregnation process was conducted using a set of hot plate tools as well as a magnetic stirrer with a heat requirement of 80 ºC and a rotation speed of 300 rpm. Chemical impregnation for each 30 g carbon sample lasted for 3 hours. Subsequently, the 0.5 M KOH impregnation sample was dried using an oven at 110 ºC for 2 days. Dry carbon powder impregnated with KOH was compressed into a solid, non-brittle monolithic coin using a hydraulic press.

Eighth, carbon coins were activated using a PayunTech Furnace Model NDT 5.2 L for opening the pore structure through one-stage integrated pyrolysis (carbonization-physical activation/N2-CO2 purchased from PT. Samator group, Indonesia).

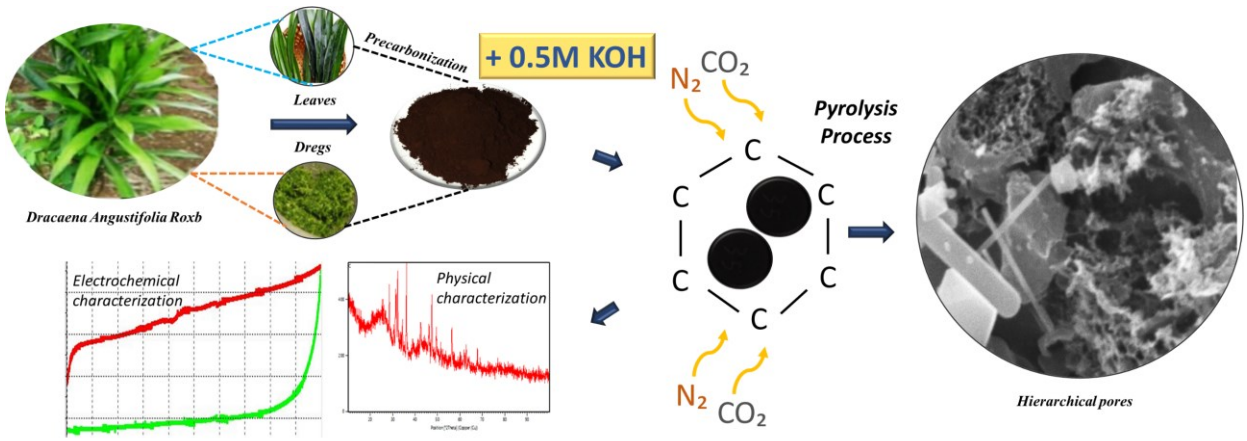

Fig. 1. Flow diagram for the experimental process of hierarchical porous activated carbon from suji waste

The carbonization process (N_2) was conducted from an initial temperature of 30-289 ºC with a gas flow rate of 1 ºC/min and held for 1 hour. In addition, N_2 carbonization was continued to completion at a temperature of 600 ºC with a gas flow rate of 3 ºC/min to remove impurities and increase carbon purity. The pyrolysis process was completed through a physical activation stage (CO_2) up to a temperature of 850 ºC which formed a carbon pore structure and increased the surface area. Ninth, the activated carbon samples of each variation were neutralized through immersion in 1000 ml distilled water to pH=7 using pH indicator strips (non-bleeding) Supelco purchased from Emsure Merck KgaA, made in Darmstadt, Germany. Tenth, the neutral activated carbon coins were re-dried using a drying oven at 110 ºC to characterize their physical and electrochemical properties.

2.2. Physical and electrochemical characterization

The effect of changes in precursor solidity was observed by measuring density loss during the pyrolysis process. This measurement employed a standard equation to estimate the density of solid carbon based on mass, diameter, and thickness measurements taken before and after pyrolysis. In addition, X-ray diffraction (XRD) was utilized to analyze the phase and degree of crystallization of the samples over the angle range (2θ) of 10° to 60°, using a Cu K-α source on the X–Pert Powder Panalytical instrument. The morphological structure of the samples was examined using a scanning electron microscope (SEM) at magnifications of 5000x and 4000x with a JEOL JSM-6510 LA. The elemental composition was determined through energy dispersion spectroscopy (EDS) using the same instrument. Subsequently, the DA porosity properties were evaluated using Quantachrome Touchwin V1.22 with the N_2 absorption technique at 77 K. The specific surface area and micropores were determined using the Brunauer–Emmett–Teller (BET) method and the Barrett-Joyner-Halenda (BJH) technique, respectively.

The performance of the DA supercapacitor was evaluated using a two-electrode configuration system, employing Cyclic Voltammetry (CV), Galvanostatic Charge Discharge (GCD), and Electrochemical Impedance Spectroscopy (EIS) techniques. Supercapacitor cell consisted of 2 solid electrodes produced by DA separated by an eggshell membrane-derived separator, with 1 M H_2SO_4 as the electrolyte. The CV method was performed using a CV UR Rad-ER 5841 physics tool with scan speeds of 1, 2, and 5 mV s^{-1}. Meanwhile, the GCD method was carried out at current densities of 1, 2, 5, and 10 A with a scan speed of 1 mV s^{-1} using CD UR Red-ER 2018. The EIS method was evaluated in the frequency range 0.01 Hz-100 Hz with a potential amplitude of 10 mV and cell voltage of 1 V. Specific capacitance (Csp), energy density (Es), power density (Pp), and resistance (ESR) were calculated using standard equations.

3. Results and Discussion

DA-based porous activated carbon was designed to be solid without adhesives in maintaining the raw material's maximum conductivity properties and improving the electrode material's performance [19]. Initial studies of material properties were conducted by measuring the sample's mass, diameter, and thickness before and after the pyrolysis process. Before the pyrolysis process, which involves carbonization and physical activation, the density values for DA dregs-KOH and DA leaves-KOH were recorded at 0.8990 g/cm³ and 0.8829 g/cm³, respectively (Fig. 2). After pyrolysis, the density of each sample decreased, with values dropping by 0.4843 g/cm³ and 0.7745 g/cm³. The pyrolysis process began with carbonization at temperatures ranging from 30 to 600°C using nitrogen (N_2) gas. This process effectively evaporated water, volatile substances, light compounds, and complex compounds such as hemicellulose, cellulose, and lignin [20]. The physical activation process was conducted using CO2 gas at temperatures reaching up to 850 °C. This process reduced tar and ash, which are by-products of carbonization, and led to the creation of an improved pore structure. The combination of these two processes results in a decrease in sample density due to the formation of high porosity. DA dregs-KOH showed the highest decrease in density followed by DA leaves-KOH, namely 46.12% and 12.27% respectively. This decrease in density was associated with the expansion of abundant pores, narrow pores, and larger pores on the surface of the DA precursor. Furthermore, these features were very useful in improving electrode interface access in supercapacitor devices. An in-depth analysis of porosity growth was reviewed in detail by carefully measuring N_2 gas absorption.

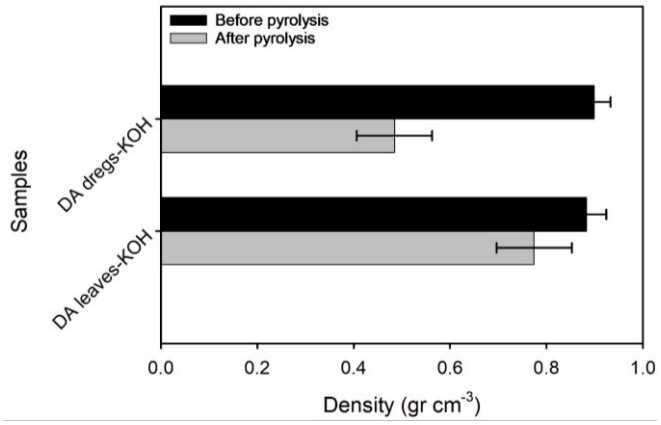

Fig. 2. Density reduction of activated carbon derived from from DA dregs - KOH and DA leaves-KOH sample

Table 1. Diffraction grating parameters for DA dregs-KOH and DA leaves-KOH

Sample	$2\theta_{002}$ (º)	$2\theta_{100}$ (º)	d_{002} (Å)	d_{100} (Å)	L_c (Å)	L_a (Å)
DA dregs-KOH	26.72	44.67	3.33	2.03	8.92	27.95
DA leaves-KOH	25.21	44.85	3.33	2.02	12.59	30.62

The XRD patterns for DA-dregs-KOH and DA-leaves-KOH were measured at a diffraction angle of 2θ (10-60)° at room temperature (25 °C). The characterization results showed two diffraction peaks in the 002 and 100 planes, namely (23-26)° and (43-46)° as shown in Fig. 3. The large (002) XRD angle at 22-26° confirmed the amorphous carbon structure that spread uniformly, random on DA aromatic samples. Meanwhile, the XRD pattern was weaker at

approximately 42-44° in the 100 plane which characterized the graphitic carbon structure. The amorphous nature observed was consistent with activated carbon materials based on biomass waste that was found previously, such as coal and fallen autumn leaves. In addition, several sharp peaks were discovered at certain angles with different intensities. This was related to the purity of carbon which bound oxygen elements to form carbon oxide [22].

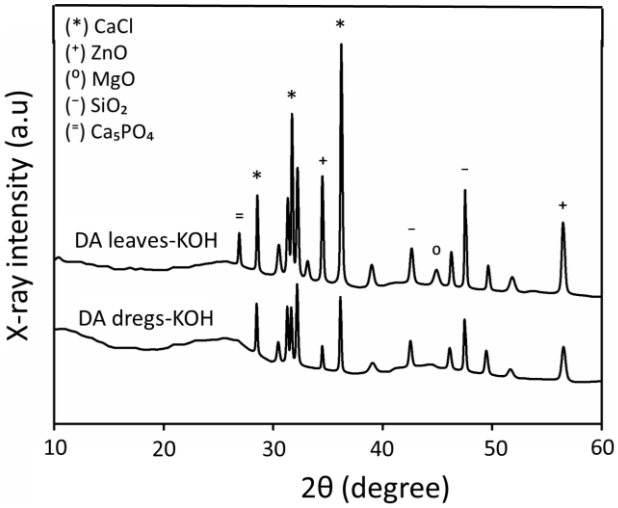

Fig. 3. XRD patterns of activated carbon from DA dregs -KOH and DA leaves-KOH samples

Scanning electron microscopy of KOH-impregnated DA dregs and DA leaves samples showed different morphological structures such as particle chunks, fiber fractures, and 3D hierarchical pores were confirmed in Fig. 4. SEM imaging was focused at 5000x and 40000x magnification, in Fig. 4(a-d). The morphological structure of the activated carbon was created by processing biomass waste from different initial conditions using KOH impregnation and pyrolysis in a nitrogen-carbon dioxide atmosphere. The KOH chemical plays a crucial role in shaping the pore structure of the activated carbon. During the pyrolysis process, which occurs at a high temperature of 850°C, a reaction takes place between KOH and the carbon. This reaction breaks the chain of organic compounds and produces gases such as CO_2 and H_2O which encourage pore formation and enlarge pore size. Fig. 4(a) presented the morphology of DA leaves-KOH from suji leaves waste at 5000x magnification with an appearance such as chunky particles and a few fibers. At 40,000x magnification (Fig. 4(b)), the fiber diameter (7-18 nm) and particle size (112-865 nm) were measured.

However, this morphology was predicted due to the influence of the presence of natural color and aromatics from the suji plant which were not completely resolved. Lack of success in evaporating color and aromatic samples could inhibit the pore formation process. Consequently, the DA leaves-KOH sample confirmed the chunky appearance of the particles. For DA dregs-KOH, 3D morphological pores were found resulting

from the treatment of reducing the color and aroma from the precursor first. This treatment was predicted to have a beneficial influence in optimizing the formation of carbon pore structures which could be used as raw material for supercapacitor electrodes [24]. The morphological structure of the DA dregs-KOH sample was focused on the 3D hierarchical pore (Fig. 4(c)). The initial treatment given to reduce natural color and aromatics from the material was an influential factor in pore formation. This 3D hierarchical structure was detected to exhibit a diameter that ranged from 520 to 1137 nm. In hierarchical pore walls, there were rich mesopores with an average diameter of <100 nm. In addition to the structure, Fig. 4(d) showed more nanofiber with fiber diameters of 21 to 46 nm. The fiber structure was produced from the natural cellulose content in the suji plant. This interconnected 3D hierarchical pore structure enhances the electrochemical performance of supercapacitor carbon electrodes by increasing material conductivity.

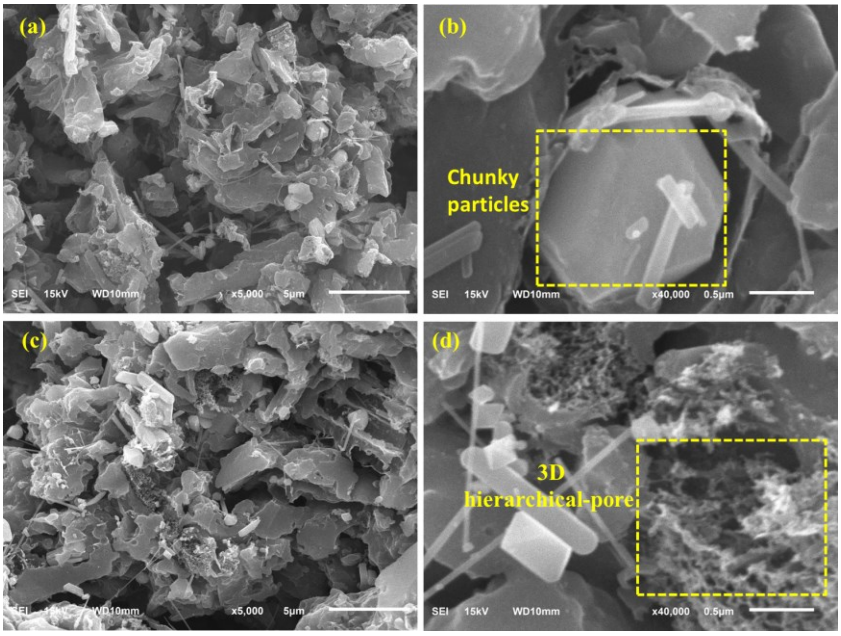

Fig. 4. Surface morphology of activated carbon samples at a magnification of (a) 5000x, (b) 40000x for DA leave-KOH (c) 5000x, and (d) 40000x for DA dregs-KOH

The composition and distribution of elements in the DA electrode were verified using the EDS, which focused on the energy range of 0 to 20 keV. Analysis showed that DA precursors had a high carbon content compared to other elements, as seen in Fig. 5(a) and 5(b). DA dregs-KOH had a higher carbon content compared to DA leaves-KOH with values of 83.59 and 78.97 % respectively. This high carbon content provided a wide range of active sites on electrode, which supported capacitive performance in supercapacitor applications [25]. Oxygen was referred to as the second most abundant element, consisting of 9.10 to 9.26% of DA composition. Meanwhile, oxygen was usually present in pyrolyzed biomass-based carbon materials, its presence was beneficial for electrode materials because it could act as doping itself, which increased the performance of supercapacitor [26]. DA solid carbon contained a small number of other elements, such as Mg, P, Si, Cl, Ca, and Zn, accounting for 0.38 to 4.67% of the total elemental composition. However, the Mg and P elements disappeared in DA dregs-KOH, showing that more pores were formed. This was explained in detail in the N_2 gas absorption analysis.

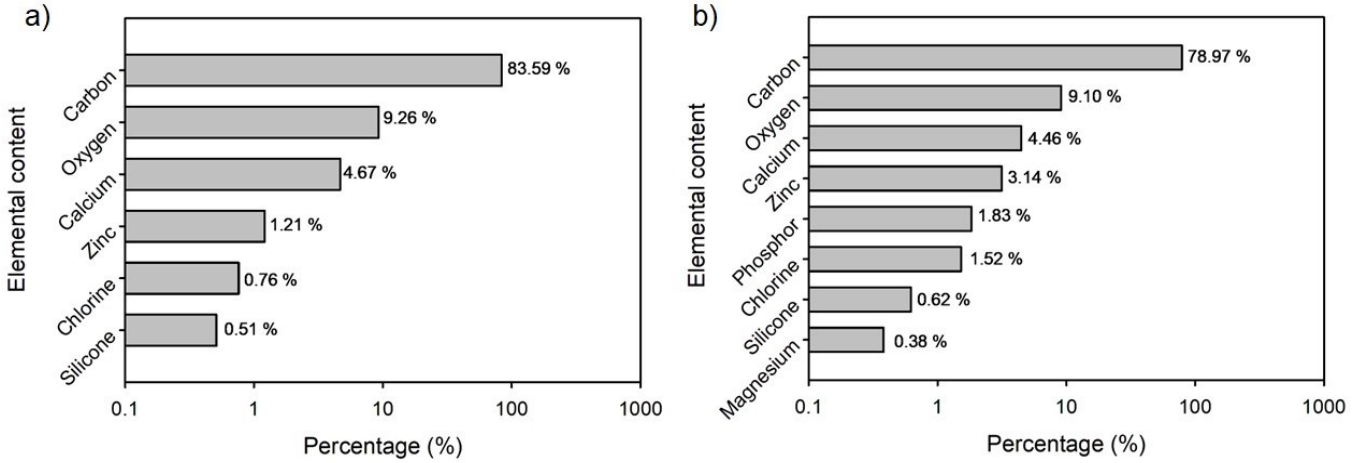

Fig. 5. Chemical composition of activated carbon from (a) DA dregs-KOH and (b) DA leaves-KOH

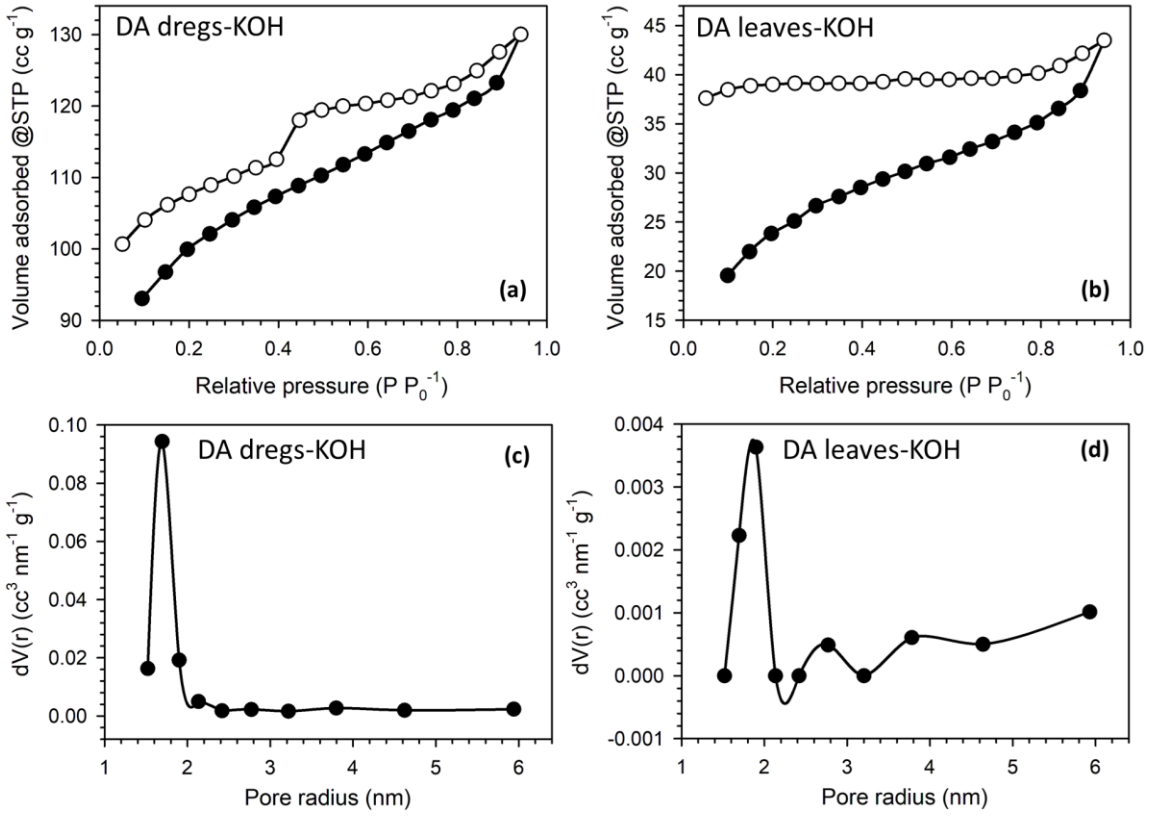

Fig. 6. (a,b) BET isotherm curve, and (c,d) pore size distribution of DA-dregs-KOH and DA leaves-KOH

The specific surface area, pore volume, and pore size distribution of DA dregs and DA leaves were measured using the isothermal N_2 adsorption-desorption method at a temperature of 77.35 K. The characterization results showed a type-IV isothermal curve which confirmed the presence of micro-mesopores. Fig. 6(a) and 6(b) revealed the DA leaves-

KOH isotherm curve with a smaller absorption volume and confirmed a smaller specific surface area of 84.32 m^2 g^{-1} using an average pore diameter of 3.198 nm. This was due to the presence of color and essential substances as natural contents of suji leaves biomass which inhibited the evaporation of lignin compounds. Consequently, the formation of pore structure from DA leaves-KOH was not optimal. The treatment of reducing natural and volatile color in DA dregs-KOH could increase the specific surface area and pore volume approximately 3 times previously to 317.66 m^2 g^{-1} and 0.2016 cc g^{-1}, as seen in Table 2 and Fig. 6(c-d). More positively, DA dregs-KOH with a high specific surface area and pore volume was showed by the availability of smaller pores with an average pore diameter of 2.534 nm. Furthermore, this significant difference in surface area values was assumed to be due to the influence of the removal of green leaves substances in the suji leaves dregs. This removal could break the chlorophyll network chain which consisted of bonds between carbon, oxygen, nitrogen, and magnesium. When the pyrolysis process was carried out on this treatment sample, it caused non-carbon elements to evaporate easily. It is known that the evaporation of non-carbon elements can produce pores that lead to the formation of porosity of AC. Where, the porosity of the material is determined by the presence and distribution of pores that can provide a large surface area with paths that can be accessed by charges. Meanwhile, a higher specific surface area is the key to the availability of sufficient space in storing ions on the electrode surface.

Fig. 6 and Table 2 shows that, the DA dregs-KOH sample confirmed a larger specific surface area value compared to the DA leaves-KOH sample [27]. This condition was characterized by a higher N_2 uptake curve with clear hysteresis loops. The hysteresis curve confirmed the availability of a greater amount of mesopores in DA dregs-KOH. It was claimed that mesopores in activated carbon could increase the power density of supercapacitor devices. Where mesopores with a 3D hierarchical structure could contribute to increasing the absorption capacity of the sample by providing a smooth transportation path for electrically charged ions filling electrode pores. Therefore, porosity and specific surface area are supporting factors for optimizing the DA dregs-KOH sample into activated carbon with the highest specific capacitance performance value.

Table 2. Surface area, volume, and pore diameter values for DA dregs-KOH and DA leaves-KOH

Sample	Morfologi	S_{BET} (m^2/g)	S_{micro} (m^2/g)	S_{meso} (m2/g)	V_{tot} (cc/g)	D_{ave}
DA leaves-KOH	Chunks of particles	84.32	15.04	69.28	0.0675	3.198
DA dregs-KOH	Hierarchical	317.66	26.91	290.75	0.2016	2.534

Electrochemical properties were measured using the CV method to determine the specific capacitance value of the activated carbon supercapacitor electrode. This measurement used a Physics CV UR Rad-ER 6841 instrument with VersaStat II Princeton Applied Study calibration, percentage error of ±6.0%. In this study, this characterization was conducted at a low potential of 0-1 V with a constant scan rate of 1 mV s^{-1}. The CV measurement curve was a relationship between current density and voltage with a curve shape such as an imperfect rectangle. Fig. 7 presented a curve show of the CV measurement results for samples of suji leaves that were with and without cooperation.

The electrochemical performance of DA dregs and DA leaves based on the effect of the addition of 0.5 M KOH chemical was measured in a symmetrical 2-electrode system. Both electrode were in a strongly acidic environment, namely 1M H_2SO_4 aqueous electrolyte at a low potential of 0-1000 mV. Generally, CV tests showed curves such as the distorted rectangles resulting from the relationship between voltage and current density. The CV test of DA dregs samples produced a wider output curve of 154 F g^{-1}, while DA leaves-KOH was only 128 F g^{-1}. In addition, in the DA dregs curve, there was a unique appearance of DA leaves, which included a more prominent curve in the charge current. This phenomenon was triggered by pseudocapacitance properties which could be seen from the spontaneous increased in current in the voltage region of 0.48-0.81V. The presence of maximum oxygen elements (self-dopping heteroatoms) as natural precursor elements could trigger the formation of oxidation-reduction reactions which supported an increase in specific capacitance. In short, oxygen doping attached to the carbon electrode matrix can integrate with electrolyte ions from H_2SO_4 through reversible electron transfer and create active sites for ion adsorption so that electrolyte ions can more easily fill the pores of the electrode surface, which of course increases the storage capacity.

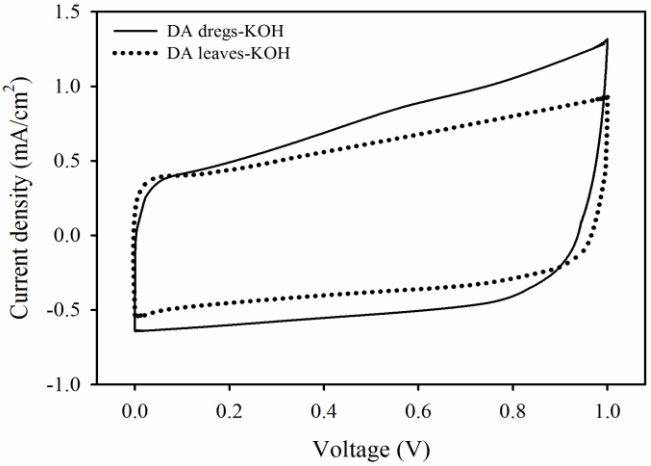

Fig. 7. Voltammetry cycle of activated carbon DA-dregs-KOH and DA leaves-KOH samples

DA dregs-KOH samples had higher electrochemical performance compared to DA leaves-KOH, showed by a wider CV curve. This analysis correlated with the smaller porosity and surface area of the treatment and the low availability of mesopores. Low mesopores result in the formation of active sites that were not optimal between electrode and electrolyte to produce better capacitance values. from DA dregs-KOH.

Further analysis of this study was shown in Fig. 7(a). and 7(b). Based on the variation of scan rate on this treatment, it was able to maintain its EDLC properties which was confirmed by the output of the CV curve showing a distorted

rectangular shape. Scan rate (1 mV s^{-1}) confirmed the oxidation-reduction process with pseudocapacitance properties from the diffusion of charged ions, which filled the DA dregs-KOH pores and resulted in higher specific capacitance values. The length of time provided for electrically charged ions to fill electrode pores showed maximum absorption. These results revealed that the appearance of electrode curve with a 3D hierarchical pore structure with the addition of a fiber structure supported the conductivity value of this treatment. Furthermore, the presence of optimal micro mesopores and high specific surface area was an added value for this treatment electrode in storing and providing smooth current during the electrochemical process. This showed a curve revealing the effect of different scan rates on specific capacitance values.

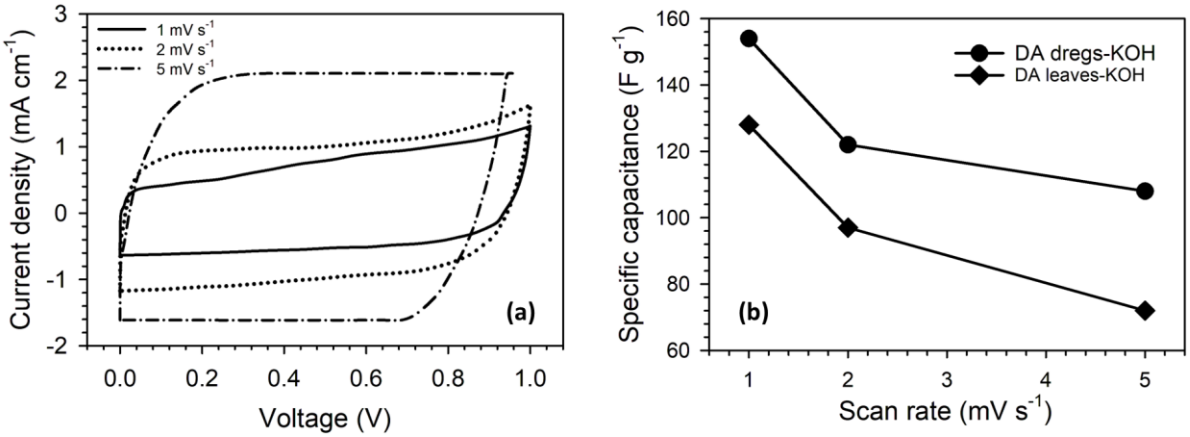

Fig. 8. (a) Voltammetry cycles and (b) specific capacitance at different scan rates from DA-dregs-KOH and DA leaves-KOH

The longer the duration required for the charging and discharging process, the greater the specific capacitance value produced [29]. The DA dregs-KOH sample revealed long charging and discharging durations, which confirmed the high specific capacitance value of 248 F g^{-1}. Meanwhile, the DA leaves-KOH sample had a smaller charging and discharging duration with a specific capacitance of 166 F g^{-1}. This was because the specific surface area of the DA dregs-KOH sample was higher than that of DA leaves-KOH. In addition, a favorable morphology was present in this treatment which supported high capacitance [30], in Table 3. Easy accessibility through active sites provided good ionic transport for supercapacitor electrodes [31]. Subsequently, its coulombic efficiency of 84.1% showed low electrolyte degradation during the charging process along with the high access of electrolyte ions to the sample. The IR dip depicted in the GCD profile was barely detectable, showing that the DA resistance was relatively low. This was due to the combination of micro and meso pores in the sample which provided ion accessibility. The Ragone plot showed the energy and power densities for both samples, as shown in Fig. 9(b). The DA dregs-KOH sample showed high energy and power densities of 12.96 Wh kg^{-1} and 148.46 W kg^{-1}.

The electrochemical behavior of DA dregs-KOH was analyzed through different electrochemical techniques, which included CV, GCD, and EIS [32]. Nyquist plot of this treatment was evaluated by EIS measurements in the frequency range of 0.01 Hz to 100 kHz, as shown in Fig. 10(a). This was performed in 2 parts in the study, at high and low frequencies. At high frequencies, it showed a semicircular curve that reflected the conductivity of material for the diffusion of electrolyte ions and was also related to the ohmic equivalent resistance (Rs) [40]. This treatment had an ohmic resistance of 0.56 Ω showing that high conductivity could be maintained. At low frequencies, there was a steep slope curve that confirmed the fast ionic diffusion capability and normal capacitive properties of supercapacitor.

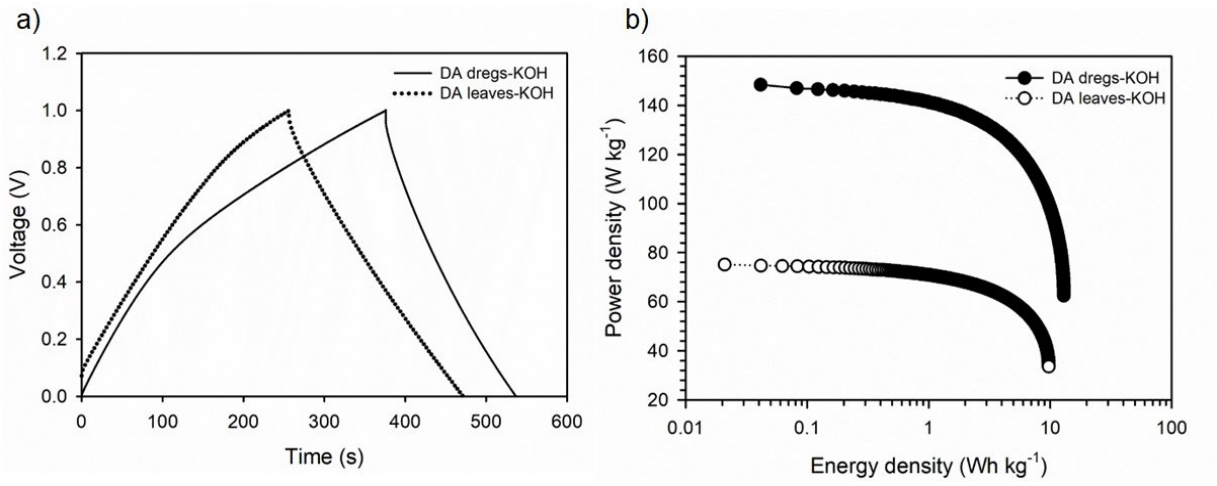

Fig. 9. (a) GCD curve. (b) Ragone plot of activated carbon DA-dregs-KOH and DA leaves-KOH

Table 3. Comparison of the electrochemical performance of different studies of porous carbon biomass-based

Biomass	Morfology structure	Carbon type	Binder material	Csp ($F\ g^{-1}$)	Esp ($Wh\ kg^{-1}$)	Ref
Eggplant	spongy porous	Powder	polytetrafluoroethylene (PTFE)	469	38.51	[30]
Chitin	hierarchical porous carbon	Powder	polytetrafluoroethylene (PTFE)	277.4	7.2	[32]
Garden biomass waste	-	Monolit	polyvinylidene fluoride (PVDF)	228	7.91	[33]
Lycium chinensis	hierarchically porous carbon	Powder	PTFE	520	12.5	[34]
Dried bamboo pulp	hierarchically porous carbon	Powder	PVA	331	10.3	[35]
Seaweed powder	3D Honeycomb	Powder	PVDF	448.3	3.125	[36]
foxtail grass seeds	hierarchically porous carbon	Powder	PTFE	358	18.2	[28]
Sword bean	hierarchically porous carbon	Powder	PVDF	369	12	[37]
corn straw	hierarchically porous carbon	Powder	PVA	269.47	15.54	[38]
Lessonia Trabeculata	highly coupled flake	Powder	PVDF	81.6	2.82	[39]
DA dregs-KOH	hierarchically porous carbon nanofiber	Monolit	Binder free	248	12.96	In this study

Two curves on the Nyquist plot showed that the DA dregs-KOH electrode produced high conductivity, low resistance, and good capacitive properties to support high-performance electrochemical supercapacitor [41]. Fig. 10(b) revealed the bode plot of this treatment confirming the pure EDLC-type supercapacitor device followed by the pseudocapacitance effect [42]. Furthermore, the capacitance of the DA dregs-KOH supercapacitor through the EIS method consisted of real capacitance (C') and imaginary capacitance (C") [43]. The curve showing the real capacitance against the applied frequency was shown in Fig. 10(c). Evaluation curve of the number of electrolyte ions reaching the interface carbon in a certain frequency region. Fig. 10(d) showed the curve of the imaginary capacitance (C″) as a function of frequency representing the relaxation time. This parameter showed the minimum time required to discharge the voltage of the device efficiently. Therefore, adsorption or desorption of the ion occurred fast on the DA dregs-KOH electrode.

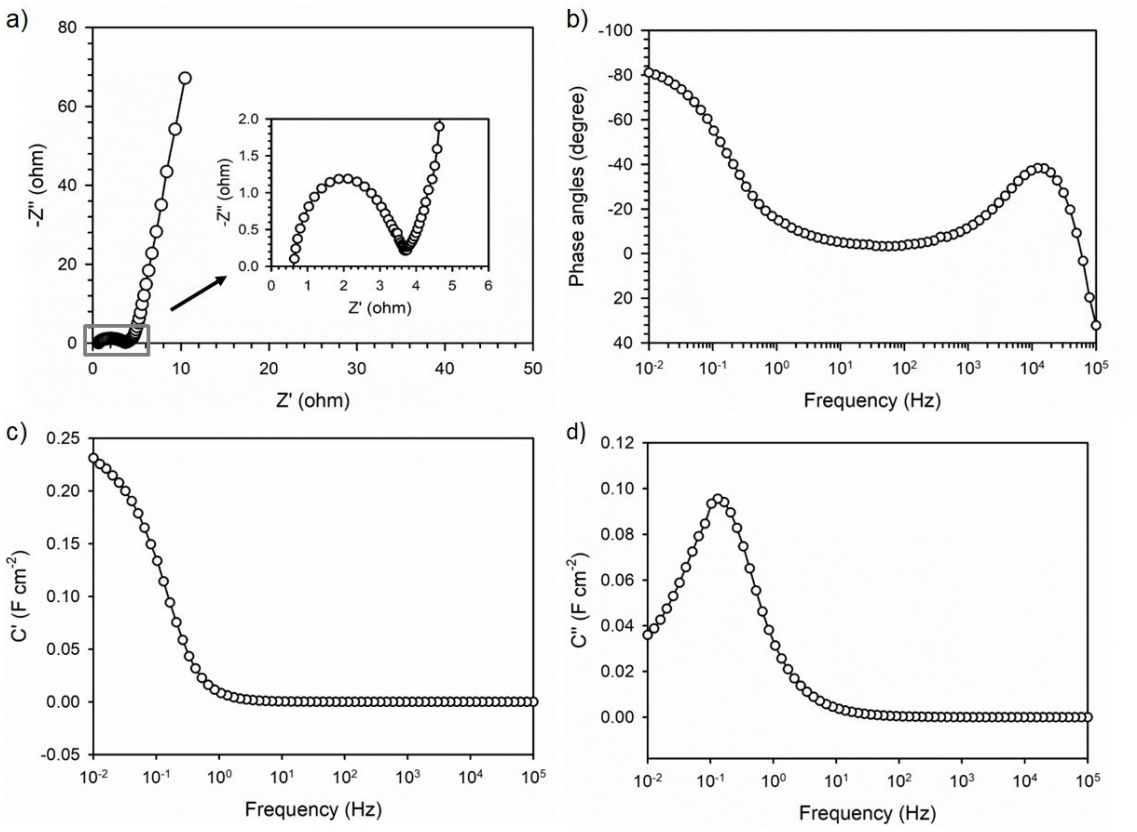

Fig. 10. (a) Nyquist plot (b) sign plot, (c) real vs. real capacitance frequency, and (d) Imaginer capacitance vs. frequency of activated carbon derived from DA-dregs-KOH and DA leaves-KOH

4. Conclusion

In conclusion, an approach using DA biomass through chemical activation and high-temperature pyrolysis produced hierarchical porous activated carbon followed by nanofiber. DA-based active carbon was obtained using 2 different treatments, namely colored DA leaves-KOH and DA dregs-KOH. DA dregs-KOH showed the highest porosity with a specific surface area of 317.66 m^2 g^{-1}. In the symmetric supercapacitor system with aqueous electrolyte, the prepared treatment electrode showed capacitances of 248 and 166 F g^{-1} at 1 A g^{-1}, respectively. Furthermore, the DA dregs-KOH electrode showed high energy and power performance, namely 12.96 Wh kg^{-1} and 148.46 W kg^{-1}. The chemical activation process and high-temperature pyrolysis maximized the potential of the color removed as carbon source with hierarchical pores followed by a nanofiber structure. The dregs of DA-KOH shows significant promise as a high-performance supercapacitor electrode material, with the potential to contribute to more sustainable and efficient energy storage solutions.

Acknowledgements

The research was financially supported by First year Project of Fundamental-Reguler (PFR) in Kementerian Pendidikan, Kebudayaan, Riset, dan Teknologi, Republic of Indonesia with the title “Gravimetric-volumetric performance enhancement of dual-cylinder supercapacitors through a combination of hierarchical-porous nanocarbon and multi-doping based on typical Indonesian aromatic biomass waste” contract No.: 20614/UN19.5.1.3/AL.04/2024.

References

1. J.J. Rico, R. Pérez-Orozco, J. Porteiro, D. Patiño, *Effect of air staging and porous inert material on the emission of volatile organic compounds in solid biomass combustion*, Fuel 351 (2023) 1–9.
2. E. Misran, O. Bani, E.M. Situmeang, A.S. Purba, *Banana stem based activated carbon as a low-cost adsorbent for methylene blue removal: Isotherm, kinetics, and reusability*, Alexandria Eng. J. 61 (2022) 1946–1955.
3. Y. Hamzah, E. Taer, A. Apriwandi, F.L. Supian, N. Mozaffari, N. Mozaffari, *Cigarette filter butts-derived activated carbon with free binder electrode design for solid-state supercapacitor application*, Commun. Sci. Technol. 8 (2023) 134–142.
4. B. Shaku, T.P. Mofokeng, N.J. Coville, K.I. Ozoemena, M.S. Maubane-Nkadimeng, *Biomass valorisation of marula nutshell waste into nitrogen-doped activated carbon for use in high performance supercapacitors*, Electrochim. Acta 442 (2023) 141828.
5. K. Yang, Q. Fan, C. Song, Y. Zhang, Y. Sun, W. Jiang, P. Fu, *Enhanced functional properties of porous carbon materials as high-performance electrode materials for supercapacitors*, Green Energy Resour. 1 (2023) 100030.
6. E. Taer, L. Pratiwi, Apriwandi, W.S. Mustika, R. Taslim, Agustino, *Three-dimensional pore structure of activated carbon monolithic derived from hierarchically bamboo stem for supercapacitor application*, Commun. Sci. Technol. 5 (2020) 22–30.
7. M. Honarmand, A. Naeimi, M.S. Rezakhani, M.A. Chaji, *Ni/NiO doped chitosan-cellulose based on the wastes of barley and shrimp for degradation of ciprofloxacin antibiotic*, J. Mater. Res. Technol. 18 (2022) 4060–4074.
8. S. Malayil, L. Loughran, F.M. Ulken, J. Satyavolu, *Exploring hemp seed hull biomass for an integrated C-5 biorefinery: Xylose and activated carbon*, J. Bioresour. Bioprod. (2024) 1–12.
9. R. Devi, V. Kumar, S. Kumar, M. Bulla, A.K. Mishra, *Performance optimization of the symmetric supercapacitors based on paddy straw-derived porous activated carbon*, J. Energy Storage 79 (2024) 110167.
10. O. Tomin, R. Vahala, M.R. Yazdani, *Synthesis and efficiency comparison of reed straw-based biochar as a mesoporous adsorbent for ionic dyes removal*, Heliyon 10 (2024) e24722.
11. D. Kasprzak, M. Galiński, *Chitin as a universal and sustainable electrode binder for electrochemical capacitors*, J. Power Sources 553 (2023) 0–9.
12. N. Izaguirre, M. Alberro, X. Erdocia, J. Labidi, *Kraft and organosolv lignin-activated carbon composites for supercapacitor electrode materials*, J. Energy Storage 80 (2024) 110386.
13. Y.Y. Minjun Kim, Xingtao Xu, Ruijing Xin, Jacob Earnshaw, Aditya Ashok, Jeonghun Kim, Teahoon Park, Ashok Kumar Nanjundan, Waleed A. El-Said, Jin Woo Yi, Jongbeom Na, *KOH - Activated Hollow ZIF - 8 Derived Porous Carbon : Nanoarchitectured Control for Upgraded Capacitive Deionization and Supercapacitor*, ACS Appl. Mater. Interfaces 44 (2021) 52034–52043.
14. Z.W. Zhang, C.Y. Lu, G.H. Liu, Y.J. Cao, Z. Wang, T. ting Yang, Y.H. Kang, X.Y. Wei, H.C. Bai, *Self-assembly of caragana-based nanomaterials into multiple heteroatom-doped 3D-interconnected porous carbon for advanced supercapacitors*, Mater. Today Adv. 19 (2023) 100394.
15. J. Zhu, J. Song, B. Han, J. Gao, Z. Liu, Y. Wang, G. Xin, *Nanoarchitectonics on residual carbon from gasification fine slag upon two step low temperature activation for application in supercapacitors*, IScience 26 (2023) 108186.
16. D. Indrasti, N. Andarwulan, E. Hari Purnomo, N. Wulandari, *Suji Leaf Chlorophyll: Potential and Challenges as Natural Colorant*, J. Ilmu Pertan. Indones. 24 (2019) 109–116.
17. S. Rashmi Manippady, M. Michalska, M. Krajewski, K. Bochenek, M. Basista, A. Zaszczynska, T. Czeppe, L. Rogal, A. Jain, *One-step synthesis of a sustainable carbon material for high performance supercapacitor and dye adsorption applications*, Mater. Sci. Eng. B 297 (2023).
18. E. Taer, N. Yanti, A. Apriwandi, A. Ismardi, R. Taslim, *Novel O , P , S self-doped with 3D hierarchy porous carbon from aromatic agricultural waste via H3PO4 activation for supercapacitor electrodes*, Diam. Relat. Mater. 140 (2023) 110415.
19. E. Taer, Apriwandi, F. Hasanah, R. Taslim, *Nanofiber-enrich activated carbon coin derived from tofu dregs as electrode materials for supercapacitor*, Commun. Sci. Technol. 6 (2021) 41–48.
20. H. Chen, Y. Guo, F. Wang, G. Wang, P. Qi, X. Guo, B. Dai, *An activated carbon derived from tobacco waste for use as a supercapacitor electrode material*, New Carbon Mater. 32 (2017) 592–599.
21. A. Gopalakrishnan, S. Badhulika, *Effect of self-doped heteroatoms on the performance of biomass-derived carbon for supercapacitor applications*, J. Power Sources 480 (2020) 228830.
22. X. Geng, G. Singh, C.I. Sathish, Z. Li, R. Bahadur, Y. Liu, S. Li, X. Yu, M. Breese, J. Yi, A. Vinu, *Biomass derived nanoarchitectonics of porous carbon with tunable oxygen functionalities and hierarchical structures and their superior performance in CO2 adsorption and energy storage*, Carbon N. Y. 214 (2023) 118347.
23. K. Al, S. Başakçılardan Kabakcı, *Oxygen-rich precursors via glycerol*

organosolv treatment: Preparation of activated carbon from hazelnut shell and its structural components for possible use in electrodes for supercapacitors, Int. J. Thermofluids 21 (2024).

24. J. Sun, A. Jayakumar, C.G. Díaz-Maroto, I. Moreno, J. Fermoso, O. Mašek, *The role of feedstock and activation process on supercapacitor performance of lignocellulosic biochar*, Biomass and Bioenergy 184 (2024).
25. N. Zhao, L. Deng, D. Luo, P. Zhang, *One-step fabrication of biomass-derived hierarchically porous carbon / MnO nanosheets composites for symmetric hybrid supercapacitor*, Appl. Surf. Sci. 526 (2020) 146696.
26. E. Taer, R. Taslim, A. Apriwandi, *Biomass-based Self-single-oxygen Heteroatom-doped Hierarchical Porous Carbon Nanosheets for High-performance Symmetrical Supercapacitors*, Chemnanomat 8 (2022) e202200217.
27. I.W. Risdianto, A. Ahmad, R.A. Ermawar, *Synthesis of cellulose acetate (CA) from algae Gracilaria sp. composited with nickel oxide (NiO) as a supercapacitor base material*, Commun. Sci. Technol. 8 (2023) 87–92.
28. X. Liang, R. Liu, X. Wu, *Biomass waste derived functionalized hierarchical porous carbon with high gravimetric and volumetric capacitances for supercapacitors*, Microporous Mesoporous Mater. 310 (2021) 110659.
29. J. Chaparro-Garnica, D. Salinas-Torres, M.J. Mostazo-López, E. Morallón, D. Cazorla-Amorós, *Biomass waste conversion into low-cost carbon-based materials for supercapacitors: A sustainable approach for the energy scenario*, J. Electroanal. Chem. 880 (2021) 114899.
30. E. Taer, N.Y. Effendi, R. Taslim, A. Apriwandi, *Interconnected micro-mesoporous carbon nanofiber derived from lemongrass for high symmetric supercapacitor performance*, J. Mater. Res. Technol. 19 (2022) 4721–4732.
31. P.M. Shafi, N. Joseph, A. Thirumurugan, A.C. Bose, *Enhanced Electrochemical Performances of Agglomeration-free LaMnO3 Perovskite Nanoparticles and Achieving High Energy and Power Densities with Symmetric Supercapacitor Design*, Chem. Eng. J. 338 (2018) 147–156.
32. J. Wang, Y. Xu, M. Yan, B. Ren, X. Dong, J. Miao, L. Zhang, X. Zhao, Z. Liu, *Preparation and application of biomass-based porous carbon with S, N, Zn, and Fe heteroatoms loading for use in supercapacitors*, Biomass and Bioenergy 156 (2022) 106301.
33. Z. Husain, S.R.A. R, K.B. Ansari, A.B. Pandit, M.S. Khan, M.A. Qyyum, S.S. Lam, *Nano-sized mesoporous biochar derived from biomass pyrolysis as electrochemical energy storage supercapacitor*, Mater. Sci. Energy Technol. 5 (2022) 99–109.
34. H. Xu, Y. Zhang, L. Wang, Y. Chen, S. Gao, *Hierarchical porous biomass-derived carbon framework with ultrahigh surface area for outstanding capacitance supercapacitor*, Renew. Energy 179 (2021) 1826–1835.
35. Y. Zhang, S. Hui, X. Lin, Z. Ying, Y. Li, J. Xie, *Novel effective strategy for high-performance biomass-based super-flexible hierarchically porous carbon fibrous film electrode for supercapacitors*, J. Alloys Compd. 883 (2021) 160713.
36. Z. Zhang, W. Yang, Y. Wu, G. Yan, L. Li, Y. Qing, X. Lu, *Porous 3D Honeycomb Structure Biomass Carbon as a Supercapacitor Electrode Material to Achieve Efficient Energy Storage*, Ind. Eng. Chem. Res. 60 (2021) 11079–11085.
37. L. Luo, L. Luo, J. Deng, T. Chen, G. Du, M. Fan, W. Zhao, *High performance supercapacitor electrodes based on B / N Co-doped biomass porous carbon materials by KOH activation and hydrothermal treatment*, Int. J. Hydrogen Energy 46 (2021) 31927–31937.
38. C. Fang, P. Hu, S. Dong, Y. Cheng, D. Zhang, X. Zhang, *Construction of carbon nanorods supported hydrothermal carbon and carbon fiber from waste biomass straw for high strength supercapacitor*, J. Colloid Interface Sci. 582 (2021) 552–560.
39. S. Sankaranarayanan, M. Hariram, S. Vivekanandhan, R. Navia, *Sustainable biocarbon materials derived from Lessonia Trabeculata macroalgae biomass residue for supercapacitor applications*, Energy Storage 3 (2021) e222.
40. B. Mei, O. Munteshari, J. Lau, B. Dunn, L. Pilon, *Physical Interpretations of Nyquist Plots for EDLC Electrodes and Devices*, J. Phys. Chem. C 122 (2018) 194–206.
41. R. Taslim, R. Refanza, M.I. Hamdy, A. Apriwandi, E. Taer, *One-step strategy of 3D hierarchical porous carbon with self-heteroatom-doped derived bread waste for high-performance supercapacitor*, J. Anal. Appl. Pyrolysis 105956 (2023).
42. C. Huettner, F. Xu, S. Paasch, C. Kensy, Y.X. Zhai, J. Yang, E. Brunner, S. Kaskel, *Ultra-hydrophilic porous carbons and their supercapacitor performance using pure water as electrolyte*, Carbon N. Y. 178 (2021) 540–551.
43. N.O. Laschuk, E.B. Easton, O. V. Zenkina, *Reducing the resistance for the use of electrochemical impedance spectroscopy analysis in materials chemistry*, RSC Adv. 11 (2021) 27925–27936.